EUROPEAN ORGANIZATION FOR NUCLEAR RESEARCH (CERN)

LHCb-INT-2013-001
January 1, 2013

Partial reconstruction of $b \to$ charm $+ \pi^+\pi^-\pi^-$ and $\overline{B}{}^0_s \to D^+_s D^-_s$ decays

Sheldon Stone, Zhou Xing and Liming Zhang

Abstract

A method of partial reconstruction is described that can be implemented in order to determine the relative momentum dependent detection efficiency ratios for K^-/K^+ and $\overline{p}/p$. Furthermore this method can be extended to modes such as $\overline{B}{}^0_s \to D^+_s D^-_s$ where large gains in the event yield may be possible.

1 Introduction

Measurement of many production and CP asymmetries are limited by our rather poor knowledge of relative detection efficiencies of charged hadrons. While the momentum dependent efficiency ratio for pions $\epsilon(\pi^+)/\epsilon(\pi^-)$ has been measured [1, 2] to be consistent with zero with an accuracy of about 0.1%, such measurements are more difficult for kaons, although work has started [3], and as yet not attempted for protons. We discuss here a strategy for adding to the kaon measurements, starting the proton determination, and potentially increasing the yields in multi-body b hadronic decays which have five or more hadronic tracks.

The basic idea is to use partial reconstruction as in the pion efficiency ratio measurement discussed above. Partial reconstruction has also been used in measuring the q^2 distribution in semileptonic b decays [4]. The procedure we outline here is somewhat different. Consider the hadronic decay of a b flavoured hadron, as shown in Fig. 1, where the b decays into three charged hadrons and charm hadron. For simplicity let us label the three charged hadrons as pions. In fact, we could have kaons as well as pions and more than three tracks. What is important is that there are a sufficient numbers of tracks to form a vertex so that the position of the b decay is accurately determined. Then the charmed hadron travels downstream and subsequently decays into a sufficient number of tracks, again three to define an accurate vertex position.

It is our contention that a sufficient number of constraints exist so that this decay can be reconstructed with one of the charm hadron decay tracks missing. Let is be specific temporarily in terms of the final state, so take $\overline{B}^0 \to D^+\pi^+\pi^-\pi^-$, $D^+ \to K^-\pi^+\pi^+$. Here as our objective is to measure $\epsilon(K^-)$ we try to reconstruct this final state both with and without detecting the K^-. Applying the same procedure to the charge conjugated final states allows determination of $\epsilon(K^+)$, and hopefully an accurate determination of $\epsilon(K^+)/\epsilon(K^-)$ as most systematic errors will cancel in the ratio.

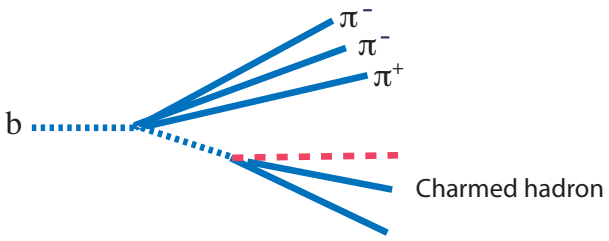

Figure 1: Sketch of a b flavored hadron decaying into a charmed hadron and 3 charge pions. The charmed particle subsequently decays into 3 charged tracks, one which indicated by the dashed red line can either be found or remain undetected.

2 Partial reconstruction procedure

It is possible to reconstruct this $\overline{B}^0$ when the K^- is missing because the decay is well over constrained. Assuming that events are selected such that the primary, $\overline{B}^0$ and D^+ decay vertices are well measured, the (c) constraints are:

- Energy and momentum (4c)
- $\overline{B}^0$ direction (3c)
- D^+ direction (3c)
- D^+ invariant mass (1c)

This gives a total of 11 constraints, not using the $\overline{B}^0$ mass subtracts one, which we need to examine for the presence of a signal. We do not know the $\overline{B}^0$ or D^+ energies, and the number of constraints lost by not detecting the kaon is three, so we have two constraints.

The fitting technique is straightforward and based on the well-known Lagrange multiplier method. The method is outlined in the Appendix.

There are several other modes that can be used with similar geometries for the kaon measurement, these include:

- $B^- \to D^0\pi^+\pi^-\pi^-$, $D^0 \to K^-\pi^+\pi^+\pi^-$,
- $\overline{B}^0_s \to D^+_s\pi^+\pi^-\pi^-$, $D^+_s \to K^+K^-\pi^+$,
- $\overline{B}^0 \to D^{*+}\pi^-$, $D^{*+} \to \pi^+D^0$, $D^0 \to K^-\pi^+\pi^+\pi^-$.

For the last reaction there is only one charged pion rather than three, so the constraint becomes the intersection point of the pion with the putative D^+ direction , which is weaker than situation discussed here by one constraint, but the $D^{*+} - D^0$ mass difference provides an additional constraint, and the total remains at two.

For the determination of $\epsilon(p)/\epsilon(\overline{p})$ the decay mode $\Lambda^0_b \to \Lambda^+_c\pi^+\pi^-\pi^-$, $\Lambda^+_c \to pK^-\pi^+$ is very promising. One simply follows the same procedure for the proton and anti-proton, by fully and partially reconstructing the decay. Any asymmetry in the kaon detection cancels in the ratio.

For measuring the K^-/K^+ and $\overline{p}/p$ efficiency ratios the resolution on the momentum of the missing hadron is important.

To estimate the resolution obtainable on the missing kaon we use data from fully reconstructed B decays in the $\overline{B}^0 \to D^+\pi^+\pi^-\pi^-$, $D^+ \to K^-\pi^+\pi^+$ decay chain. After selecting these events we ignore the kaon. The momentum resolution of the missing kaon after using the specific procedure discussed in the Appendix is shown in Fig. 2. This resolution is similar to that found for the missing pion in $D^{*+} \to \pi^+D^0$, $D^0 \to K^-\pi^+\pi^+\pi^-$ decays, where one of the pions from the D^0 is missed [2].

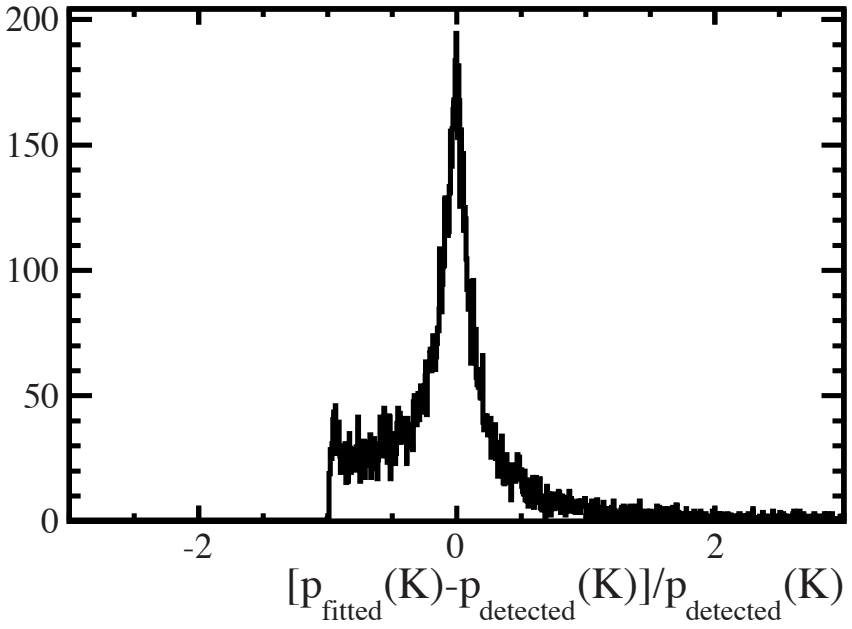

Figure 2: The inferred kaon momentum resolution in 2011 data.

3 Enhancing $\overline{B}{}^0_s \to D^+_s D^-_s$

It is also interesting to apply these ideas to other decays where there is one particle that is not detected. We use the example of the $\overline{B}{}^0_s \to D^+_s D^-_s$ decay. This mode could be very interesting; with sufficient statistics it provides an alternative place to measure lifetimes and *CP* violation, as it is a *CP* even eigenstate.

Consider that as a baseline the $D^\pm_s \to K^+K^-\pi^\pm$ decays. The $\overline{B}{}^0_s$ decay can be reconstructed, in principle, if there is one missing track in either of the D_s decays. The gain here is quite large. The detection of efficiency of a single track in a typical B decay is approximately 0.7, for the track required to be between $10 - 400$ mrad of the beam. If we need to detect only five out of the six tracks present in the decay then the efficiency is increased from $(0.7)^6$ to $6(0.7)^5$, the ratio giving an increase of a factor of 8.6. A minor modification of the technique described above is necessary as the $\overline{B}{}^0$ decay point is given by the intersection of the two D_s directions. This reduces the number of constraints by one, on the other hand there is an additional D_s mass constraint, so again the total number of constraints remains at two.

It will also be necessary to consider relevant backgrounds. Some of these backgrounds can be enlisted to provide signal. Consider for example the case where the $D^+_s \to K^+K^-\pi^+\pi^0$. This branching fraction is almost the same size as the $K^+K^-\pi^+$ mode. The decay one D_s can be reconstructed with the additional π^0 in the same manner as for a

missing charged track. It could provide a factor of 4 increase in the number of events.[1] Another potential background source is the decay $\overline{B}^0 \to D_s^* D_s$. This decay can also be looked for using the fitting technique. In fact it could produce a nice increase in signal yield, perhaps a factor of three, and here there are three additional constraints.

The important consideration here is the $\overline{B}$ mass resolution. Follow the method in the Appendix we find the inferred mass resolution for $\overline{B}^0 \to D^+\pi^+\pi^-\pi^-$, $D^+ \to K^-\pi^+\pi^+$ decays shown in Fig. 3. A triple Gaussian function has been used to fit the B mass resolution distribution, $\Delta m(B)$, the narrow Gaussian component (38%) has a width of 49 MeV while the intermediate one 157 MeV (41%) and wide one 456 MeV (21%).

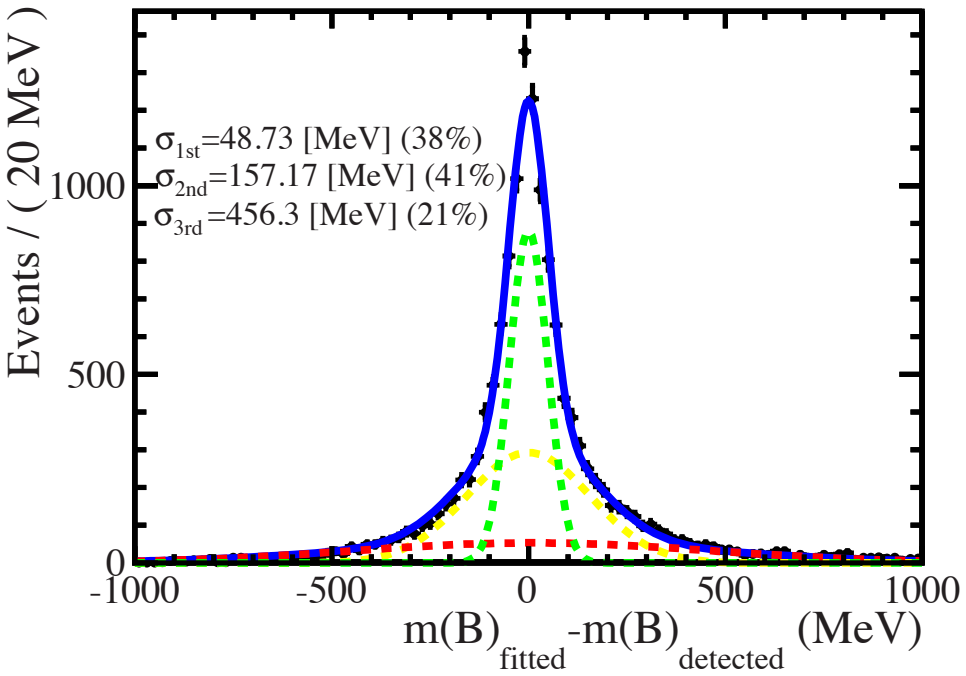

Figure 3: The inferred B mass resolution in 2011 data.

This resolution should be good enough to utilize this technique. We also note that the resolutions can be improved by imposing tighter cuts on the vertex resolution and flight distance.

4 Conclusions

We have proposed several uses of partial reconstruction including measuring the relative K^+/K^- and $p/\overline{p}$ detection efficiencies and perhaps increasing the yields in $\overline{B}_s^0 \to D_s^+ D_s^-$ and related modes. Other applications of these techniques surely exist.

[1] Other D_s decay modes can also be considered.

References

[1] LHCb collaboration, M. Artuso *et al.*, *Measurement of the $D_s^+ - D_s^-$ Production Asymmetry*, LHCb-ANA-2012-011. .

[2] LHCb collaboration, R. Aaij *et al.*, *Measurement of the $D_s^+ - D_s^-$ production asymmetry in 7 TeV pp collisions*, Phys. Lett. **B713** (2012) 186, arXiv:1205.0897.

[3] M. Vesterinen, *Kaon asymmetry corrections for a_{sl}^s*, Talk at semileptonic working group meeting, Nov. 7, 2012.

[4] LHCb collaboration, M. Artuso *et al.*, *Measurement of b-hadron production fractions in 7 TeV centre-of-mass energy pp collisions* , LHCb-ANA-2011-065. ; LHCb Collaboration, R. Aaij *et al.*, *Measurement of b-hadron production fractions in* 7 TeV pp *collisions*, Phys. Rev. **D85** (2012) 032008, arXiv:1111.2357.

Appendix: Fitting technique and expected resolutions

The constraint equations are

$$|\vec{p}(B^0)|\hat{n}_x(B^0) = \vec{p}_x(3\pi) + |\vec{p}(D^+)|\hat{n}_x(D^+) \tag{1}$$

$$|\vec{p}(B^0)|\hat{n}_y(B^0) = \vec{p}_y(3\pi) + |\vec{p}(D^+)|\hat{n}_y(D^+) \tag{2}$$

$$|\vec{p}(B^0)|\hat{n}_z(B^0) = \vec{p}_z(3\pi) + |\vec{p}(D^+)|\hat{n}_z(D^+) \tag{3}$$

$$|\vec{p}(D^+)|\hat{n}_x(D^+) = \vec{p}_x(2\pi) + \vec{p}_x(K) \tag{4}$$

$$|\vec{p}(D^+)|\hat{n}_y(D^+) = \vec{p}_y(2\pi) + \vec{p}_y(K) \tag{5}$$

$$|\vec{p}(D^+)|\hat{n}_z(D^+) = \vec{p}_z(2\pi) + \vec{p}_z(K) \tag{6}$$

$$\sqrt{|\vec{p}(D^+)|^2 + m^2_{PDG}(D^+)} = E(2\pi) + \sqrt{\vec{p}_x{}^2(K) + \vec{p}_y{}^2(K) + \vec{p}_z{}^2(K) + m^2_{PDG}(K)} \tag{7}$$

where $\hat{n}(B^0) = \vec{n}(B^0)/|\vec{n}(B^0)|$, with $\vec{n}(B^0) = \vec{x}(B^0) - \vec{x}(PV)$ indicates the the flight direction of B^0 from PV (primary vertex) to secondary B^0 vertex and $\hat{n}(D^+) = \vec{n}(D^+)/|\vec{n}(D^+)|$ with $\vec{n}(D^+) = \vec{x}(D^+) - \vec{x}(B^0)$. The 3π and 2π notation stands for the combination of pion daughters from B decay and from D decay, respectively. The mass $m(K)$, $m(D^+)$ are all constrained to their PDG values.

Using matrix notation we re-write these constraints as:

$$H(\eta, z) = 0 \tag{8}$$

where η is a 17×1 matrix that contains 17 measured variables: $x-y-z$ coordinates of secondary B^0 vertex, $x-y-z$ coordinates of secondary D^+ vertex, $p_x(3\pi)$, $p_y(3\pi)$, $p_z(3\pi)$, $E(3\pi)$, $p_x(2\pi)$, $p_y(2\pi)$, $p_z(2\pi)$, $E(2\pi)$ and $x-y-z$ coordinates of primary vertex. z is a 5×1 matrix that contains 5 unknown variables: $|\vec{p}(D^+)|$, $|\vec{p}(B^0)|$, $\vec{p}_x(K)$, $\vec{p}_y(K)$ and $\vec{p}_z(K)$.

We define auxiliary matrices

$$D = \partial H(\eta, z)/\partial\eta \ \ (7 \times 17 \text{ matrix}) \tag{9}$$
$$E = \partial H(\eta, z)/\partial z \ \ (7 \times 5 \text{ matrix}) \tag{10}$$
$$V_D = (DV_{\eta^0}D^T)^{-1} \ \ (7 \times 7 \text{ matrix}) \tag{11}$$
$$V_E = (E^T V_D E)^{-1} \ \ (5 \times 5 \text{ matrix}) \tag{12}$$
$$d = -(D\eta + Ez) \text{ d matrix } (7 \times 1 \text{ matrix}) \tag{13}$$
$$\lambda_0 = V_D(D\eta_0 + d) \text{ Lagrange multiplier } (7 \times 1 \text{ matrix}) \tag{14}$$
$$\lambda = \lambda_0 + V_D E z \tag{15}$$

The χ^2

$$\chi^2 = \lambda^T V_D^{-1}(\lambda) \tag{16}$$

is computed iteratively until a satisfactory convergence is achieved ($\Delta\chi^2 < 0.001$). When updating in each iteration both the measured variables η and unknown variables z are updated by new states with

$$\eta = \eta_0 - V_{\eta_0} D^T \lambda \tag{17}$$
$$z = z_0 - V_E E^T \lambda_0 \tag{18}$$

along with their covariance matrices.

Some sanity checks and optimization studies have been done in MC to improve the missing particle's momentum resolution. We first take the fully reconstructed MC signals with selections shown in Table 1 applied, and then ignore the Kaon track and refit the D vertex with only information from the two pion tracks. The invariant mass distributions of the fully reconstructed B and D candidate in signal MC are shown in Fig. 4 after background category requirement and MC matching. They are both fitted with a double Gaussian function with the effective mass resolution shown on the plot.

The η matrix then consist of the refitted D vertex coordinates as well as other measurable quantities, denoted as: $\eta = \{x_D, y_D, z_D, p_x(2\pi), p_y(2\pi), p_z(2\pi), E(2\pi), x_B, y_B, z_B, p_x(3\pi), p_y(3\pi), p_z(3\pi), E(3\pi), x_{PV}, y_{PV}, z_{PV}\}$. We then examine the pull distribution of the η column vector updated by the kinematic fitter, denoted as η_f, which is defined by comparing to the initially assigned measured η vector, denoted as η_i:

$$\text{pull} = \frac{\eta_i - \eta_f}{\sqrt{\sigma_i^2 - \sigma_f^2}} \tag{19}$$

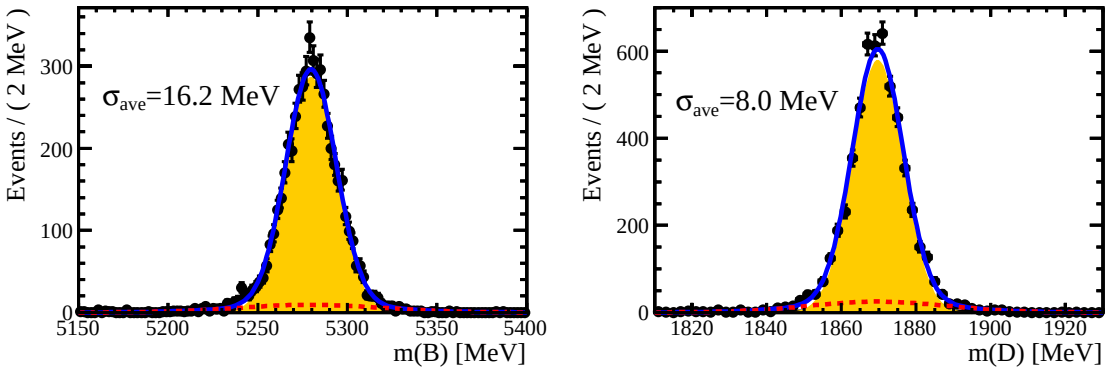

Figure 4: The invariant mass distributions of the fully reconstructed B and D candidate in signal MC.

Table 1: Selections in MC for fully reconstructed $B^0 \to D^-(K^+\pi^-\pi^-)\pi^+\pi^-\pi^+$

Item	Requirement
Background category	=10
MC matching	require match of true ID of each track and mother particles
B mass window	± 40 MeV
D mass window	± 20 MeV

where the σ_i is the initial uncertainty of measurements and σ_f the error propagated through by the fitter. Such pull distributions are shown in Fig. 5 and fitted with a Gaussian function.

Different ways of initialization of the unknown variables, z vector = $\{$ $|\vec{p}(B^0)|$, $|\vec{p}(D^+)|$, $\vec{p}_x(K)$, $\vec{p}_y(K)$, $\vec{p}_z(K)$ $\}$, are used from the measured variables η vector. $|\vec{p}(B^0)|$ can be computed in 3 different ways with a linear solution:

$$|\vec{p}(B^0)| = \frac{p_x(3\pi)\hat{n}_z(D) - p_z(3\pi)\hat{n}_x(D)}{\hat{n}_x(B)\hat{n}_z(D) - \hat{n}_z(B)\hat{n}_x(D)} \tag{20}$$

$$|\vec{p}(B^0)| = \frac{p_y(3\pi)\hat{n}_z(D) - p_z(3\pi)\hat{n}_y(D)}{\hat{n}_y(B)\hat{n}_z(D) - \hat{n}_z(B)\hat{n}_y(D)} \tag{21}$$

$$|\vec{p}(B^0)| = \frac{p_x(3\pi)\hat{n}_y(D) - p_y(3\pi)\hat{n}_x(D)}{\hat{n}_x(B)\hat{n}_y(D) - \hat{n}_y(B)\hat{n}_x(D)} \tag{22}$$

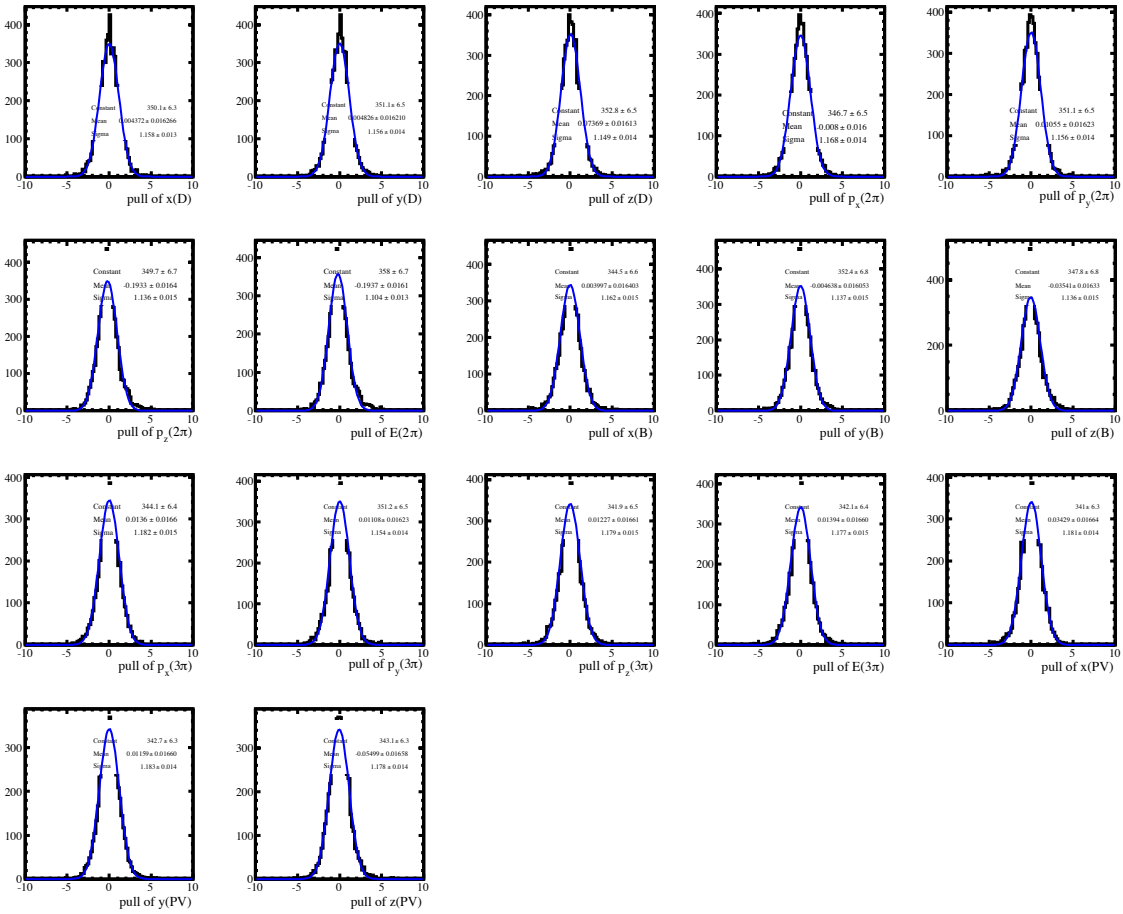

Figure 5: Pull distributions for the measurable quantities, η_f, which are updated by the kinematic fitter (MC).

and subsequent $|\vec{p}(D^+)|$ can be computed as:

$$|\vec{p}(D^+)| = \frac{|\vec{p}(B^0)|\hat{n}_x(B^0) - \vec{p}_x(3\pi)}{\hat{n}_x(D^+)} \tag{23}$$

$$|\vec{p}(D^+)| = \frac{|\vec{p}(B^0)|\hat{n}_y(B^0) - \vec{p}_y(3\pi)}{\hat{n}_y(D^+)} \tag{24}$$

$$|\vec{p}(D^+)| = \frac{|\vec{p}(B^0)|\hat{n}_z(B^0) - \vec{p}_z(3\pi)}{\hat{n}_z(D^+)}. \tag{25}$$

In principle, there can be 9 different ways to compute the initial values for $|\vec{p}(B^0)|$ and $|\vec{p}(D^+)|$, and for each combination the other 3 unknown variables, $\vec{p}_x(K)$, $\vec{p}_y(K)$ and $\vec{p}_z(K)$ are computed using Eq. 4, Eq. 5 and Eq. 6, respectively. Each one of the 9 sets of

initializations of z vector is selected to start the kinematic fitting until the kinematic fit converges, if the 9 step fitting still fails ($\sim 5\%$ events), the Eq. 22 and Eq. 25 are assigned as default for the final solution of the unknown variables in z vector.

The pull distributions of the unknown variables $|\vec{p}(B^0)|$, $|\vec{p}(D^+)|$, $\vec{p}_x(K)$, $\vec{p}_y(K)$ and $\vec{p}_z(K)$ in z vector are shown in Fig. 6 where the pull is defined as $(z_{\rm fitted} - z_{\rm measured})/\sigma(z_{\rm fitted})$ with $\sigma(z_{\rm fitted})$ as the error computed by the fitter. The same distributions are also examined for $m(B) = ((\sqrt{p(D)^2 + m^{PDG}(D)^2} + E(3\pi))^2 - p(B)^2)^{1/2}$, $p(K) = \sqrt{p_x(K)^2 + p_y(K)^2 + p_z(K)^2}$ and $p_T(K) = \sqrt{p_x(K)^2 + p_y(K)^2}$ in Fig. 6. There is a broad component in the pull distribution, this is caused by the facts that the initial values for η and z vector can sometimes be heavily smeared off the true values since B and D vertices (unlike the PV), and thus the D flight direction are not well measured, and also the quadratic constraint Eq. 7 can sometimes cause the fitter to pick up the wrong unphysical solution during the minimization. All the pull distributions are fitted by double Gaussian functions.

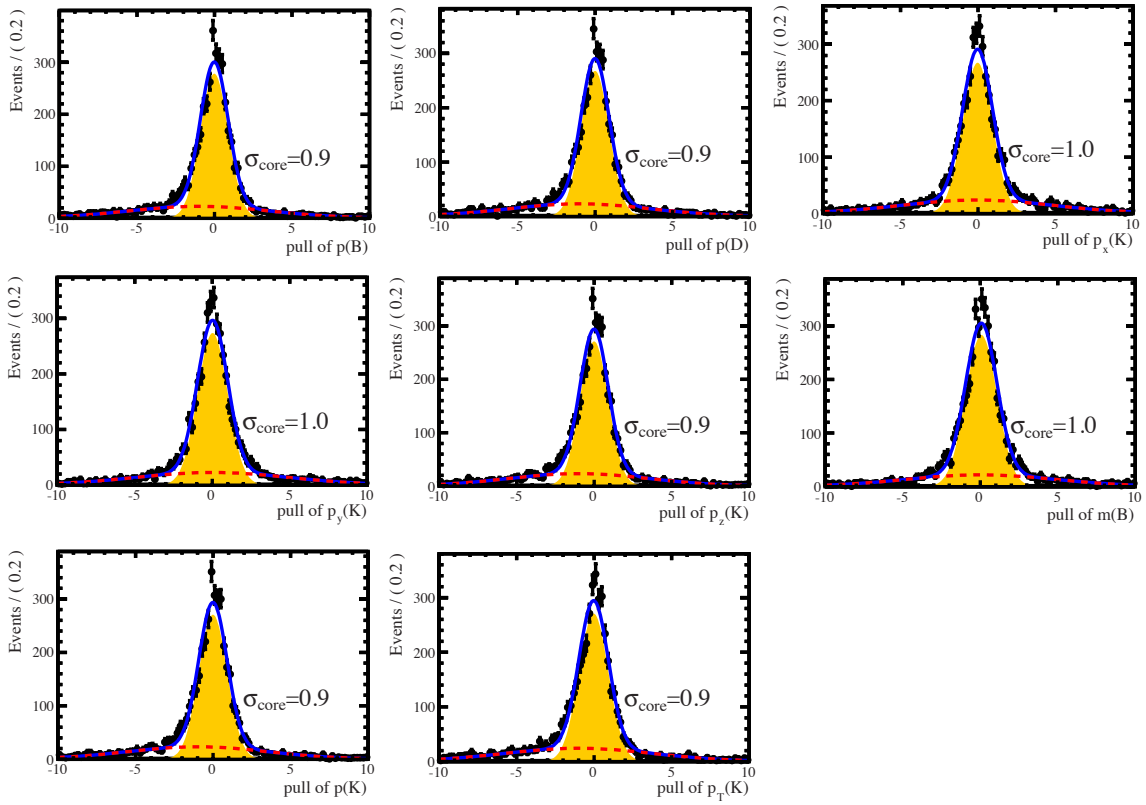

Figure 6: Pull distributions for the fitted unknown variables (MC).

We check that, when only replacing the measured B and D vertices (6 variables) in η vector for initialization by their corresponding MC true values, the tails are removed in the pull distributions .

Table 2: Selections, in data, for fully reconstructed $B^0 \to D^-(K^+\pi^-\pi^-)\pi^+\pi^-\pi^+$

Item	Requirement
D^- meson	$\pm 20\,\text{MeV}$ mass window
$a_1(3\pi)$ vertex fit	$\chi^2/NDF < 6$
Kaons and pions	Kaon PIDK> 4
	Pion PIDK< 0
	$p > 2\,\text{GeV}$ and $p_\text{T} > 0.3\,\text{GeV}$
B meson	$DIRA > 0.99994$, $\chi^2_{IP} < 20$
	$\chi^2_{FD} > 100$, vertex fit $\chi^2/NDF < 8$

Having tuned up the fitting procedure on simulation, we now turn to 2011 data. Here we first fully reconstructed $B^0 \to D^-(K^+\pi^-\pi^-)\pi^+\pi^-\pi^+$ decay with selections shown in Table 2 and then refit the D^- vertex with the kaon ignored (only 2011 magnet up data is used).

Invariant mass distribution of the B meson is shown in Fig. 7 with signal region highlighted by the black vertical bars, low mass sideband region the red vertical bars and high mass sideband region the blue vertical bars. When showing distributions of any variables, the average of the low mass and high mass sideband is subtracted off the primary distribution in the signal region.

The sideband subtracted pull distributions of the unknown variables $|\vec{p}(B^0)|$, $|\vec{p}(D^+)|$, $\vec{p}_x(K)$, $\vec{p}_y(K)$ and $\vec{p}_z(K)$ in z vector, and $m(B)$, $p^{\text{inferred}}(K)$ and $p_T^{\text{inferred}}(K)$ are shown in Fig. 8 which are similar to the ones observed in simulation.

The fully reconstructed B mass distribution is fitted in the range of [5200, 5400] MeV to obtain the B mass resolution in data (17.0 MeV).

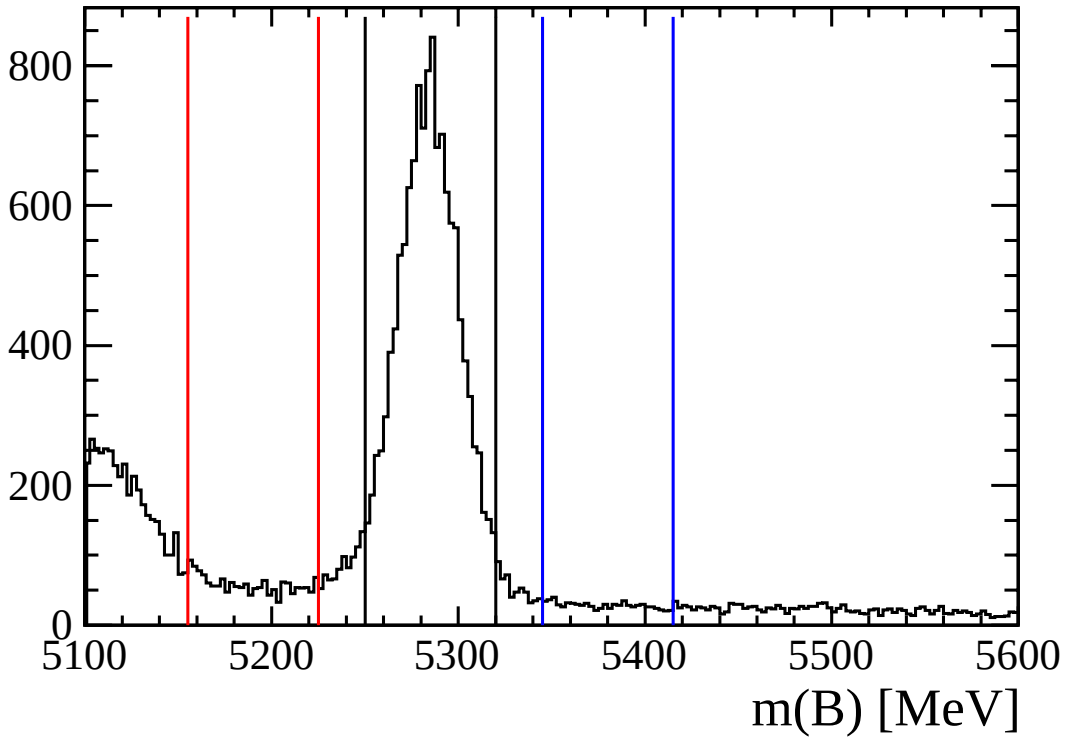

Figure 7: Invariant mass distribution of the fully reconstructed B candidate in data.

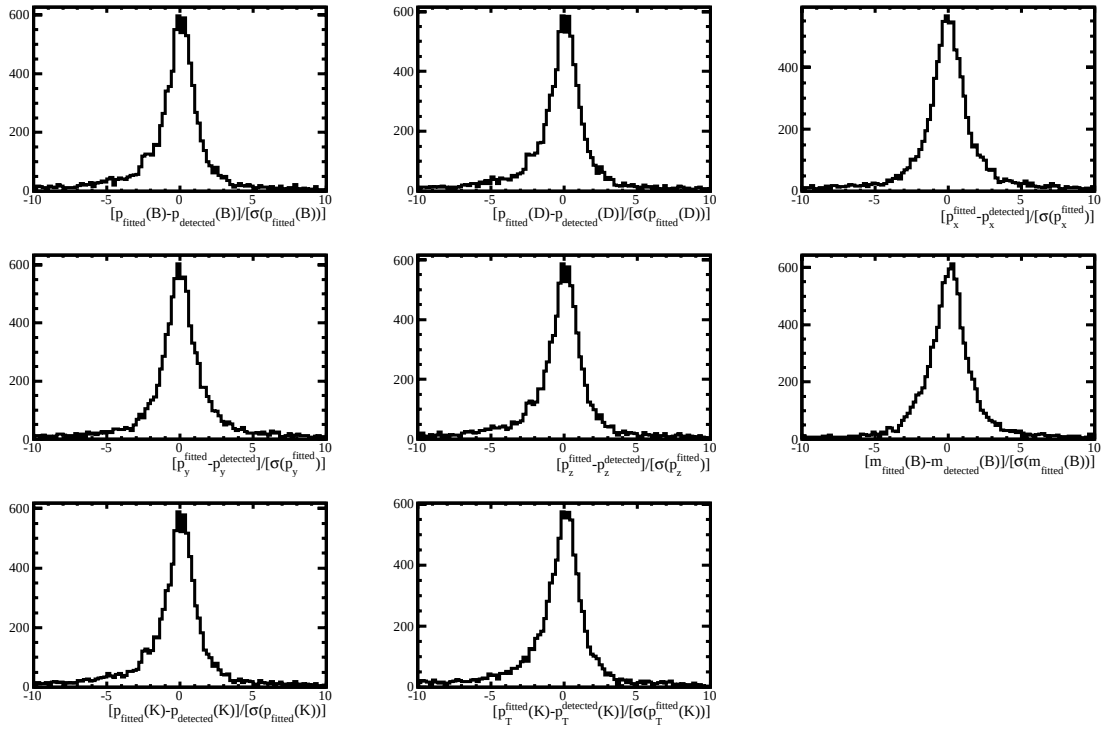

Figure 8: Sideband subtracted pull distributions for the fitted unknown variables in data.